



On the PEO treatment of cold sprayed 7075 aluminum alloy and its effects on mechanical, corrosion and dry sliding wear performances thereof

Yuqin Rao^a, Qun Wang^{a,*}, Daisuke Oka^b, Chidambaram Seshadri Ramachandran^c

^a College of Materials Science and Engineering, Hunan University, Changsha, Hunan 410082, PR China

^b Plasma Giken Co. Ltd., Toda, Saitama 369-1214, Japan

^c Department of Materials Science and Engineering, The State University of New York at Stony Brook, New York 11794 2275, USA



ARTICLE INFO

Keywords:

Cold spray
7075 aluminum alloy
Plasma electrolytic oxidation
Corrosion
Sliding wear

ABSTRACT

The plasma electrolytic oxidation (PEO) process was used to deposit an alumina coating on a cold sprayed 7075 aluminum alloy to improve the surface properties. The phase compositions, microstructures, basic mechanical properties, as well as the corrosion and the dry sliding wear resistance of cold sprayed 7075 aluminum alloy before and after PEO treatment, were investigated. The results show that a single-layered dense alumina coating with a thickness of ~15–20 μm and hardness of 1353 HV_{0.01} is realizable on the cold sprayed 7075 aluminum alloy by PEO treatment aided by an aluminate electrolyte. The corrosion current density and wear rate of the alumina PEO coating were 6.27×10^{-7} A/cm² and 1.22×10^{-6} mm³/N·m respectively, which were three and two orders of magnitude lower compared to the uncoated rolled 7075 aluminum alloy (T6) substrate, thus highlighting the excellent wear and corrosion resistance of the PEO treated cold sprayed Al alloy surface.

1. Introduction

Cold spray (CS) is an emerging and innovative additive manufacturing procedure [1,2]. In the cold spray process, the metallic/alloyed particles are accelerated by a stream of supersonic gas flow and then deposited onto the substrate under certain pressure and temperature. The sprayed particles also undergo severe plastic deformation [3]. Compared to the conventional thermal spray processes, the risk of oxidation, phase transformations, and excessive thermal stresses can be effectively reduced, since the powder particles remain in the solid-state during the cold spray deposition [4]. CS can be employed to deposit various pure metals and their alloys, such as Al [5], Cu [6], Ti [7], etc., to name a few. CS has been applied to convalesce the surface functionalization of parts used in many fields for providing adequate protection against high-temperature corrosion, oxidation, chemical reactions, etc. [8]. With the improvement of the CS technique in recent years, especially the advent of HPCS (high-pressure cold spray) systems, the employment of CS has been extended to surface reclamation, restoration, and bulk manufacturing as well [9,10]. Using HPCS, the damaged components can be repaired instead of replacing them, and free-standing components with complex structures can be fabricated. In addition to this, HPCS is favorable for building a solid construction on un-weldable base materials, in which case the substrate can remain unaltered and remain as a structural member [11]. Given the

manufacturing features of cold spray, it has found great potential for the production of components having rotational symmetry, such as flange [6], cylinder wall [10], and sputter target [12]. CS is especially suitable for the development of novel products, in which case small-scale production is usually involved. Since the CS has advanced rapid prototyping capabilities, the cost for designing and producing cast and extrusion molds will be substantially reduced/eliminated thereby improving the economics of the process. Because small-sized and light-weighted engines are favored, in recent years, to achieve reduction of fuel consumption and improvement of engine efficiency, the aluminum alloys having low densities can be utilized in manufacturing engine components like cylinder walls, to replace cast iron. Aluminum and its alloys have been proved to be viable for bulk manufacturing by the CS process since there are many research articles available in the open literature that investigate the microstructure and mechanical properties of a variety of CS Al alloys [13–17]. Bulk mechanical properties of CS deposited Al alloys have been widely studied by researchers focusing on mechanical performance tests, which showed favorable strength and hardness results. The mechanical properties of cold sprayed materials can be remarkably improved further by utilizing proper heat treatments [17–21]. The 7075-aluminum alloy has been comprehensively used in many fields, such as automotive, aerospace, and aviation industries, because of its high strength-to-weight ratio [22–24]. CS fabricated 7075 aluminum alloy with acceptable mechanical properties can be an

* Corresponding author.

E-mail address: wangqun72@163.com (Q. Wang).

alternative, especially to improve surface conditions/features/to prolong the life of other Al-alloy structures [25]. Among the most useful surface treatment techniques, the Plasma Electrolytic Oxidation (PEO) has long been utilized for generating hard ceramic coatings to protect aluminum and other alloys [26–29]. Many researchers have reported that the wear and corrosion resistance of aluminum alloys can be significantly enhanced by PEO treatment, which is attributed to the formation of the protective ceramic coating on the substrate surface enabled by the plasma discharges, supported by an aqueous electrolyte [30–33]. PEO coatings on aluminum alloys formed in aluminate electrolytes are mainly composed of Al_2O_3 [34]. The chemical stability, high hardness, and compactness of alumina coatings are the main reasons for the adequate protection against wear and corrosion. The research papers mentioned above are mainly focused on the PEO coatings formed on traditional wrought substrates. However, the literature on the employment of PEO as a surface modification technique on CS additively manufactured aluminum alloy is scant. The purpose of this study is to investigate the electrochemical corrosion and dry sliding wear performances of cold sprayed 7075 aluminum before and after modifying the surfaces by the PEO technique. The results of this paper may be instructive for the production of corrosion and wear-resistant aluminum flange that is additively sprayed on an aluminum pipe. This CS deposited, and PEO treated flange can be the right candidate for usage in friction wheels of a textile loom machinery. A set of rolled 7075 aluminum bulk substrates in T6 condition were also tested for comparison.

2. Experiment

2.1. Materials

The feed-stock used in this investigation was a gas-atomized 7075 aluminum powder (Plasma Giken. Co., Ltd., Japan) with an average diameter of 35 μm . This powder was sprayed on a 7075-aluminum substrate using high-pressure cold spray equipment (PCS-1000, Plasma Giken. Co., Ltd., Japan). The morphology and diameter distribution of the feedstock powder are shown in Fig. 1. Helium was used as the process gas to accelerate the feedstock powder to obtain critical impact velocity for effective deposition. The pressure and temperature of helium were maintained at 2 MPa and 500 °C at the heater exit during the spray process. The nozzle to substrate stand-off distance was 30 mm, the deposition angle was kept at 90°, the powder feed rate was 30 g/min, and the traverse speed of nozzle during spraying was 300 mm/s. A 10 mm thick coating deposit was made on a 5 mm thick rolled 7075 aluminum bulk substrate in T6 condition using the parameters mentioned above. Besides this, the fractional elemental composition of the cold sprayed and the rolled 7075 aluminum alloy was evaluated by X-ray fluorescence (Niton® XL3p, Thermo Fisher Scientific, USA) and listed in Table 1.

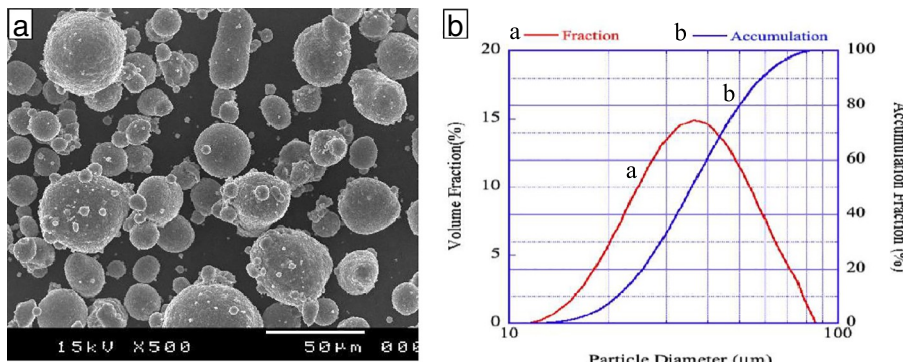


Fig. 1. (a) morphology of feedstock powder; (b) particle diameter distribution of feedstock powder.

2.2. PEO treatment

Before the PEO treatment, the cold sprayed specimens ($20 \times 10 \times 10 \text{ mm}^3$) were sectioned-off using a Wire cut Electrical Discharge Machine (WEDM). The samples thus obtained were all cold sprayed material, i.e. free-standing coatings, since the substrate used for deposition was completely removed. Each free-standing sample was connected to a copper wire and then mounted in epoxy resin to provide a $20 \times 10 \text{ mm}^2$ working surface. The working surface was ground with successive grades of abrasive SiC papers up to 1200 grit, followed by polishing with diamond emulsion. The polished samples were washed with ethanol and distilled water. The power was supplied through a 15 kW pulsed power source (JCL-DL15, Jinchuang Technology Co., Ltd., Chengdu, China). During the PEO process, a constant current setting (positive current: 0.5 A and negative current: 0.3 A) was used. Except for voltage (The voltage increased from 0 V to 400 V rapidly, followed by a gradual increase to ~ 550 V, and it stabilized at this voltage after ~ 4 min), other electrical parameters were kept constant. The processing time was 10 min, the duty cycle was 20%, and the frequency was 2000 Hz. The anode was the specimen, and the cathode was a stainless steel plate. The composition of the electrolyte was 8 g/L NaAlO_2 , 1 g/L KOH, 2 g/L EDTA-2Na, and 2 g/L $\text{Na}_3\text{C}_6\text{H}_5\text{O}_7 \cdot 2\text{H}_2\text{O}$.

2.3. Microstructure and phase composition examination

The surface and cross-sections of the PEO coatings, their morphologies before & after corrosion and wear tests were examined using an environmental scanning electron microscope (SEM; FEI Quanta 200; FEI Co., Ltd., Netherlands), equipped with energy dispersive spectroscopy (EDS). Wear scars on Al_2O_3 balls that were inspected using an optical microscope (Taiming Optical Instrument Co. Ltd.; Shanghai, China). A Miniflex 600 X-ray diffraction system (XRD; Rigaku Co., Ltd., Japan) was used to characterize phase composition of the PEO coatings (Cu K α radiation, accelerating voltage 40 kV, current 15 mA, scanning speed 20°/min, step size 0.02° and scan range from 10° to 80°).

2.4. Electrochemical corrosion tests

Electrochemical corrosion tests (ASTM G59 - 97) were carried out in a naturally aerated 3.5% NaCl (mass fraction) solution, using an electrochemical workstation, with a 3-electrode configuration. In this set-up, the specimen was the working electrode, a platinum plate was used as the counter electrode, and a saturated calomel electrode was used as the reference electrode (CHI 604D, Chen-Hua Instruments Co. Ltd., Shanghai, China). The corrosion resistance of the cold sprayed, and the rolled 7075 aluminum alloy with and without PEO coatings were evaluated by potentiodynamic polarization method. The surfaces of the uncoated samples were prepared in the same manner as discussed in Section 2.2, whereas the coated samples were only washed by deionized water and dried by warm air. The specimens were immersed in a 3.5%

Table 1
Elemental fraction of the cold sprayed and the rolled 7075 aluminum alloy.

Elemental fraction (wt%)	Al	Zn	Mg	Cu	Si	Cr	Fe	Mn	Ti
Cold sprayed 7075 Al	90.29	5.40	2.11	1.56	0.22	0.24	0.06	0.01	0.07
Rolled 7075 Al (T6)	89.77	5.65	2.12	1.43	0.20	0.25	0.28	0.09	0.09

Table 2
Mechanical properties of as-sprayed 7075 aluminum alloy.

Results	Mechanical properties	Ultimate tensile strength (MPa)	Microhardness (HV _{0.3})	Density (g/mm ³)	Elongation at fracture
Present work	Cold sprayed 7075 Al	395 ± 48	144 ± 3	2.78	2.9%
	Rolled 7075 Al	496 ± 12	179 ± 2	2.8	8.1%
Rokni et al. [18]	Cold sprayed 7075 Al	~415 ± 6	120 ± 6	–	3.2%

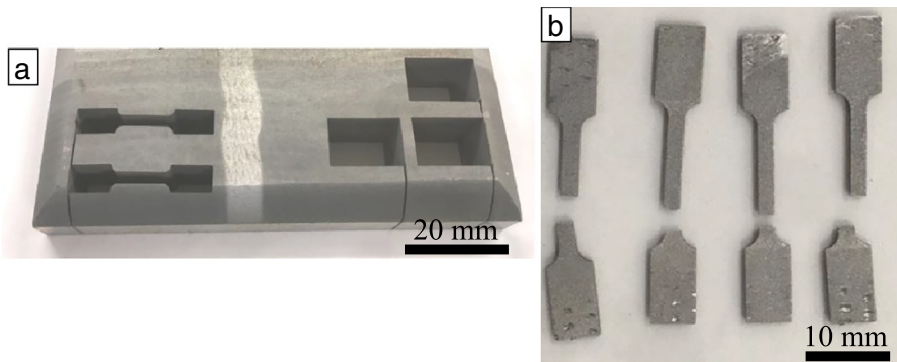


Fig. 2. (a) As-sprayed material after WEDM; (b) Cold sprayed material after tensile strength tests.

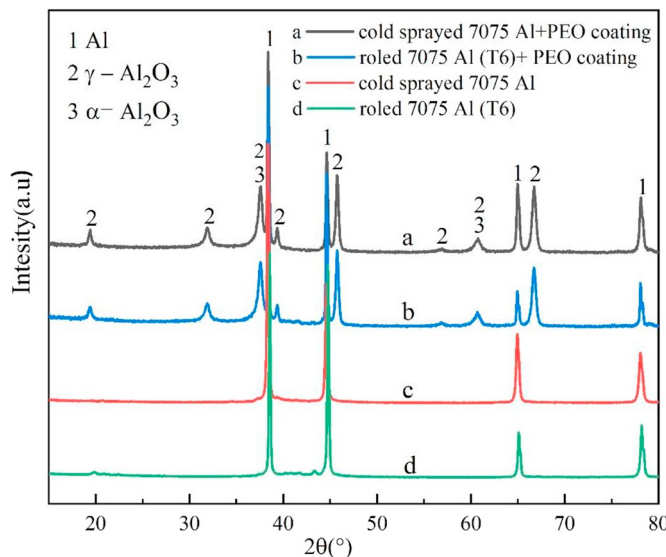


Fig. 3. XRD patterns for 7075 aluminum alloys with and without PEO treatment.

NaCl solution for 30 min to obtain open circuit potential (OCP) between working and reference electrodes. The polarization scans were started at 500 mV below the OCP and continued up to 1500 mV above the OCP with a scan rate of 1 mV/s. Three samples were tested for each condition to ensure the repeatability.

2.5. Dry sliding wear tests

The dry sliding wear tests of 7075 aluminum alloy with and without PEO coatings were performed using a ball-on-disk HT-1000 tribometer

(Zhongke Kaihua Technology Co., Ltd., Lanzhou, China) under dry conditions at a temperature of 25 °C and relative humidity of 50–55% (ASTM G99-17). A 6 mm-diameter Al₂O₃ ball was used as a counter body. Before starting the wear test, the test samples were gently ground with sequential grades of abrasive SiC papers up to a 1500 grit, followed by polishing with diamond emulsion. The polished samples were washed with ethanol and distilled water. The coating surface, thus polished, had a roughness of ~2.56 μm (Ra). During the wear test, a normal load of 5 N was applied, the sliding velocity was 100 mm/s, and the total sliding time was 7200 s. Three separate samples were subjected to dry sliding wear testing for each of the 7075 aluminum alloy with and without PEO coating.

2.6. Mechanical and metallurgical characterization tests

The ultimate tensile strength test of the as-sprayed free-standing material was carried out using an Instron 3369 uniaxial tensile tester (Plasma Giken Co. Ltd., Saitama, Japan; ASTM E8/E8M-09). The density of as-sprayed free-standing 7075 aluminum alloy was measured by Archimedes' principle. Also, the indentation method was used to test the cross-section hardness of the 7075 Al alloy and their PEO coatings with a load of 10 g and dwell time of 15 s on the HX-1000TM/LCD microhardness tester (ASTM E8/E8M-09). The results of the hardness were reported from the standard deviation of ten measurements. The bond strength of the PEO coating/substrate was evaluated using a modified ASTM C-633 test method. The cylindrical sample (Φ16 mm) was adhered to the dual pair using E-7 glue. The tensile tests were carried out with a strain rate of 1 mm/min in a universal testing machine (Instron-3382; Instron Co. Ltd., Boston, USA).

3. Results and discussion

3.1. Mechanical properties of the cold sprayed 7075 aluminum alloy

The mechanical properties of the as-sprayed 7075 aluminum alloy,

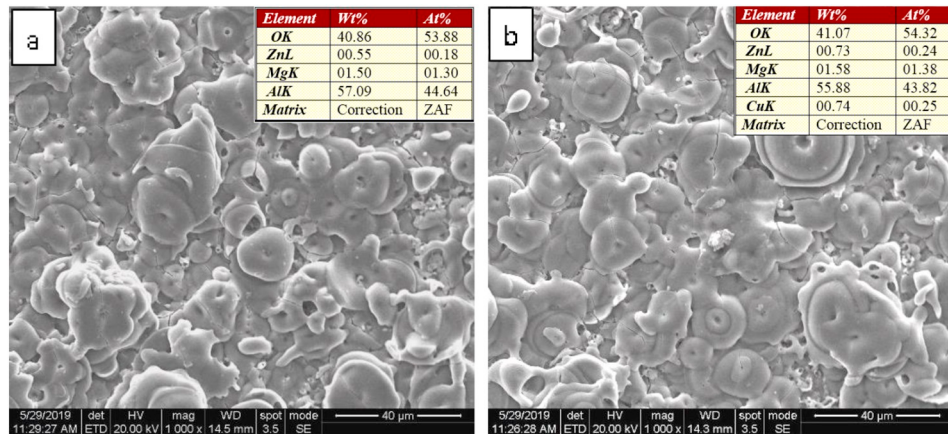


Fig. 4. SEM images (secondary electron images) showing surfaces of PEO coatings: (a) formed on the cold sprayed 7075 aluminum; (b) formed on the rolled 7075 aluminum.

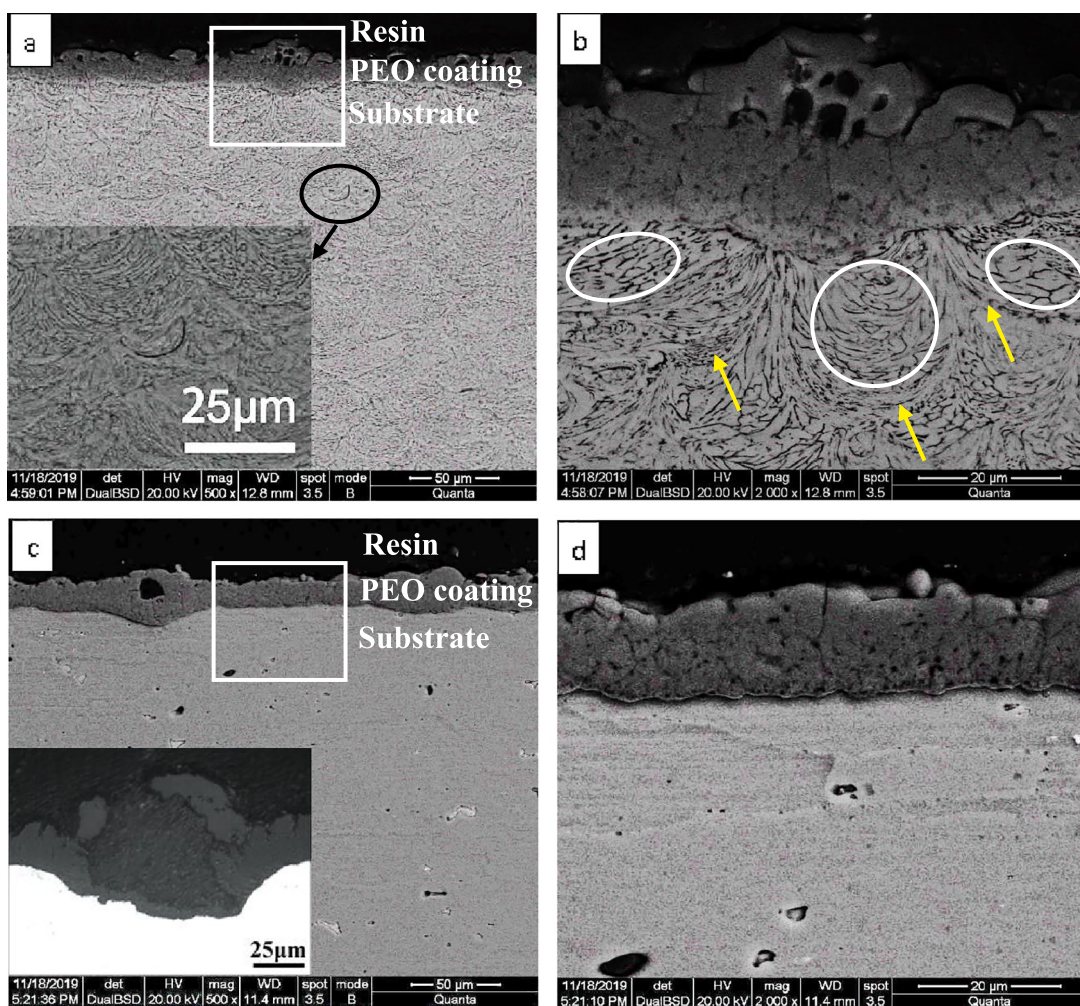


Fig. 5. SEM images (backscattered electron images) showing cross section of PEO coatings: (a, b) formed on the cold sprayed 7075 aluminum; (c, d) formed on the rolled 7075 aluminum.

and the results of Rokni et al., are listed in Table 2 for comparison. The result of the ultimate tensile strength test of the as-sprayed free-standing material shows that an average value of 4 experiments was 395 MPa. The elongation at fracture was only 2.9% (the images of the as-sprayed material after WEDM and samples after tensile strength tests are shown in Fig. 2). The microhardness of as-sprayed 7075 aluminum alloy was (144 ± 4) HV_{0.3}. Rokni et al. [18] also examined the

mechanical properties of as-deposited 7075 aluminum, and they obtained an ultimate tensile strength value of ~ 415 MPa, a microhardness of 120 ± 6 HV_{0.3}, and the elongation at fracture was $\sim 3.2\%$. The differences in the results for cold sprayed material shown in Table 2 might have originated from the different feed powders, cold spray parameters, and hardware used in the respective investigations. Also, the as-sprayed 7075 aluminum alloy in our present work exhibited an

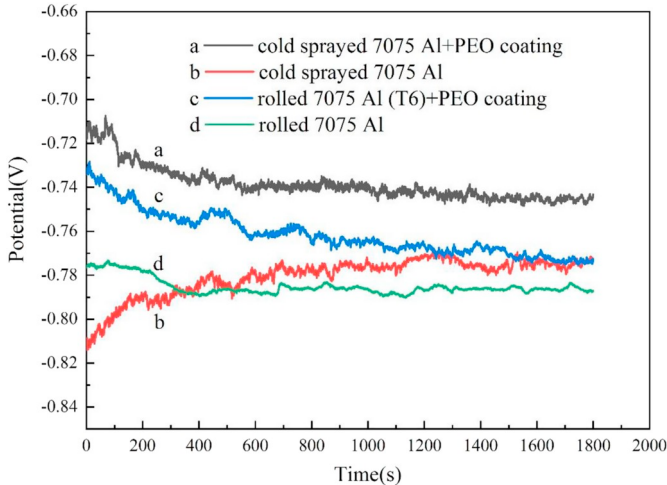


Fig. 6. OCP-time responses recorded in 3.5 wt.% NaCl solution for uncoated and coated 7075 aluminum alloy.

impressive density of 2.78 g/cm^3 , and extremely low porosity of 0.24 Vol%, without any heat treatment. Hence, the coating possesses exceptional deposit quality, and it has the potential to be effectively used in the as-sprayed condition.

3.2. Phase composition and microstructure of PEO coating

The XRD patterns for the cold sprayed, and the rolled 7075 aluminum alloy before and after PEO treatment are presented in Fig. 3. The phase compositions of the two PEO coatings were similar, with the presence of $\gamma\text{-Al}_2\text{O}_3$ as the primary phase and $\alpha\text{-Al}_2\text{O}_3$ as a minor phase. Furthermore, there was no discernible difference in the XRD results of the PEO coated samples, and the existence of sharp peaks of Al in the XRD patterns suggested that the coatings were penetrable by the X-ray.

Table 3

Results of electrochemical corrosion obtained from Fig. 7 for coated and uncoated 7075 aluminum alloys.

Sample	$E_{corr}(\text{V})$	$I_{corr}(\text{A}/\text{cm}^2)$	$R_p(\Omega\text{-cm}^2)$
Cold sprayed 7075 Al + PEO	-0.699	6.27×10^{-7}	3.90×10^4
Cold sprayed 7075 Al	-0.781	1.16×10^{-4}	6.45×10^2
Rolled 7075 Al (T6) + PEO	-0.711	2.33×10^{-6}	1.55×10^4
Rolled 7075 Al (T6)	-0.747	3.19×10^{-5}	1.87×10^3

Fig. 4 (a) and (b) display the surface morphologies of PEO coatings, in which, typical pancake structures with diameters of $\sim 10 \mu\text{m}$ can be observed clearly. The surfaces were rough with visible microcracks and micropores. The EDS results of the PEO coatings are presented in the upper right corner of Fig. 4, which shows the presence of principal elements, namely the Al, O, and traces of other alloying elements. The Al_2O_3 coatings formed on the cold sprayed alloy, and the rolled alloy displayed similar surface morphologies and chemical compositions. The cross-sectional morphologies of the PEO coatings are presented in Fig. 5, and the substrates were etched with Keller reagent. The higher magnification images of boxed areas in Fig. 5 (a) and (c) are provided on the right side. The coatings exhibited a dense single-layered structure with a thickness of $\sim 15\text{--}20 \mu\text{m}$, with few micropores and microcracks. The layer formed on the cold sprayed alloy was slightly thicker and more compact with fewer defects. The inset SEM image in Fig. 5(a) presents a poor bonded area between the CS deposited particles. The inset optical image in Fig. 5(c) shows a large crater shape defect in the PEO coating deposited on a rolled 7075 aluminum alloy, and the layer was also undesirably thin. There was no evidence of similar defects in the PEO deposited on the CS sample. The interface of the PEO coating/CS deposit was not as clear compared to that of PEO coating/rolled material. In the near-interface zone, there were distinct regions in Fig. 5(b), including the particle interiors (white circles) and particle-particle boundaries (yellow arrows). This indicates that the particles near the interface were partially consumed to form alumina during the PEO process. The microhardness measurements were made on the

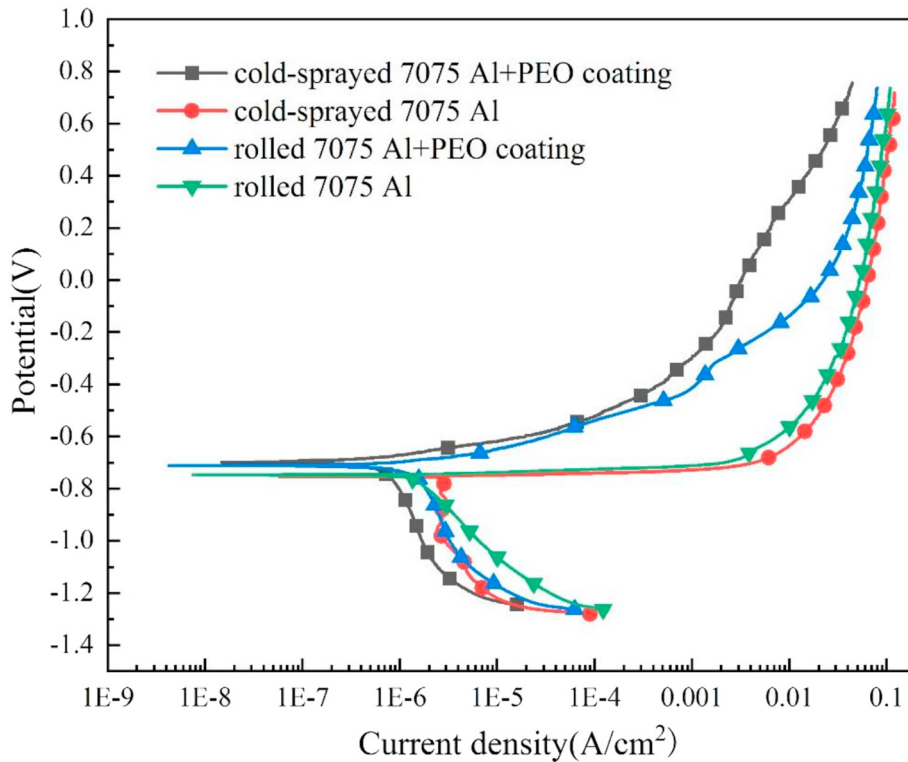


Fig. 7. Potentiodynamic polarization curves recorded in 3.5 wt% NaCl solution after OCP tests for uncoated and coated 7075 aluminum alloys.

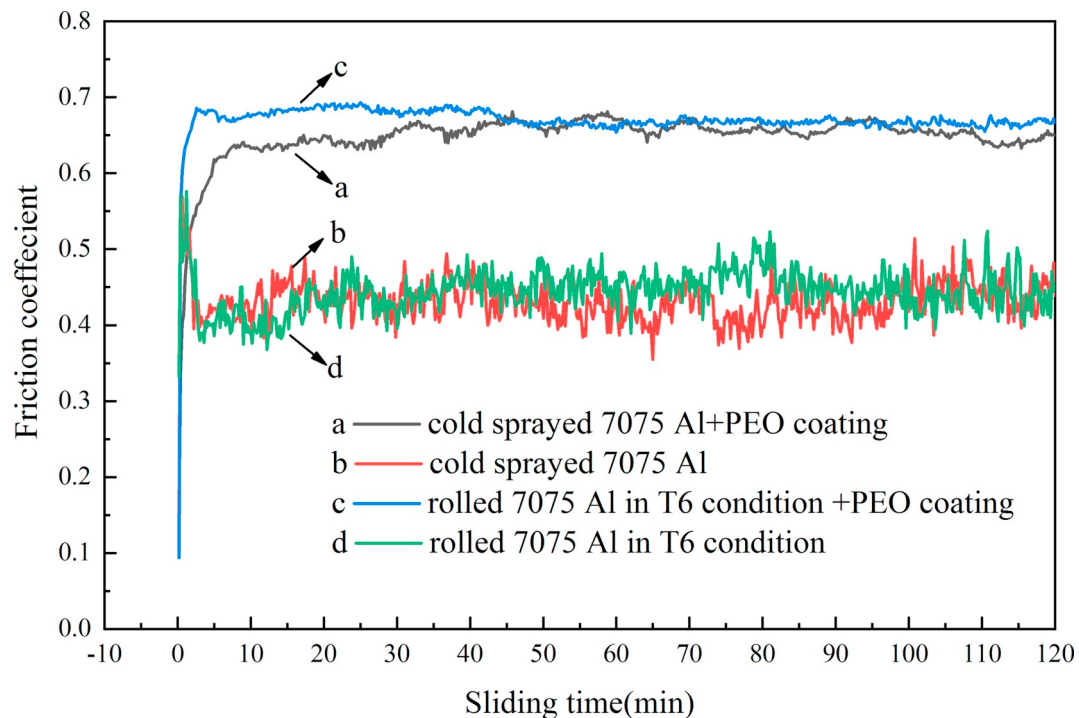


Fig. 8. Coefficient of friction as a function of sliding time under 5 N for uncoated and coated 7075 aluminum alloy.

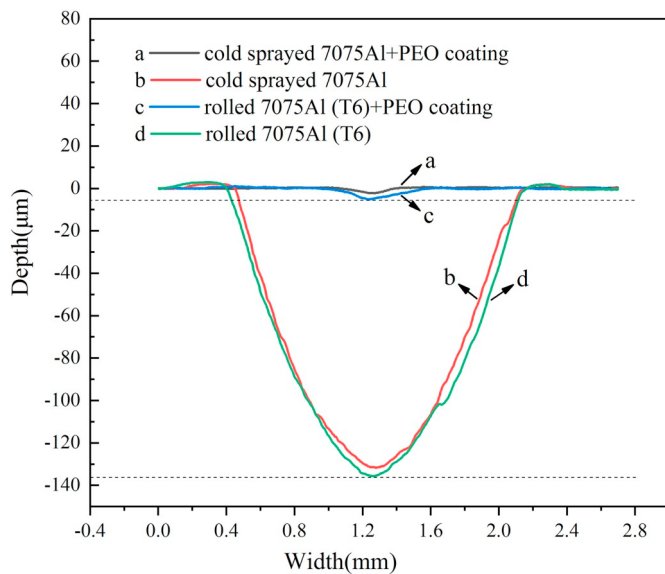


Fig. 9. Cross-sectional profiles of wear scars after dry sliding tests under a load of 5 N.

Table 4

Average coefficient of friction and wear rates of 7075 aluminum alloy with and without PEO coatings.

Sample	Coefficient of friction	Wear rate (mm ³ /N·m)
Cold sprayed 7075 aluminum + PEO coating	0.65 ± 0.04	1.22 × 10 ⁻⁶
Cold sprayed 7075 aluminum	0.43 ± 0.03	3.65 × 10 ⁻⁴
Rolled 7075 aluminum (T6) + PEO coating	0.67 ± 0.03	3.30 × 10 ⁻⁶
Rolled 7075 aluminum (T6)	0.44 ± 0.03	4.21 × 10 ⁻⁴

cross-sections of the coatings. The average hardness values of the PEO coatings deposited on the cold sprayed and rolled alloys were $1353 \pm 156 \text{ HV}_{0.01}$ and $1193 \pm 98 \text{ HV}_{0.01}$, respectively. These hardness values are found to be lying in between the hardnesses of the $\alpha\text{-Al}_2\text{O}_3$ phase (2100–2200 HV) and the cubic $\gamma\text{-Al}_2\text{O}_3$ phase (800–900 HV) respectively [35]. The bond strength between the PEO coatings and substrates were found to be exceeding 38 MPa, and the separation took place at the glue/coating boundary each time without delamination of the coatings.

3.3. Corrosion resistance

The OCP curves of the samples with and without PEO coatings are displayed in Fig. 6, which were recorded while immersing the samples in 3.5 wt% NaCl solution at room temperature for 1800 s. It is observed from Fig. 6 that fluctuations could be seen on all the curves, while the curve of the rolled 7075 aluminum alloy without coating was relatively smoother. Small variations for this sample suggest that there were fewer activation sites for localized corrosion to occur in comparison to the cold sprayed one. Those fluctuations can be treated as electrochemical noise (EN) and can be explained by the occurrence of localized and repeated corrosive actions on the surface of the samples [36,37]. Besides this, all the curves became almost stable after about 600 s, and the OCP values were found to end between -0.79 V to -0.74 V . Compared to the coated samples, the OCP values of the uncoated counterparts were found to be in a relatively negative level during the whole immersion process, implying that there is an improvement in the corrosion resistance of the 7075 aluminum alloys after PEO treatment. The curves generated during the potentiodynamic polarization test carried out in the NaCl corrosive media post OCP stabilization is displayed in Fig. 7. The corrosion current density (I_{corr}), the corrosion potential (E_{corr}), and the polarization resistance values of the samples obtained from Fig. 7 are summarized in Table 3. It is

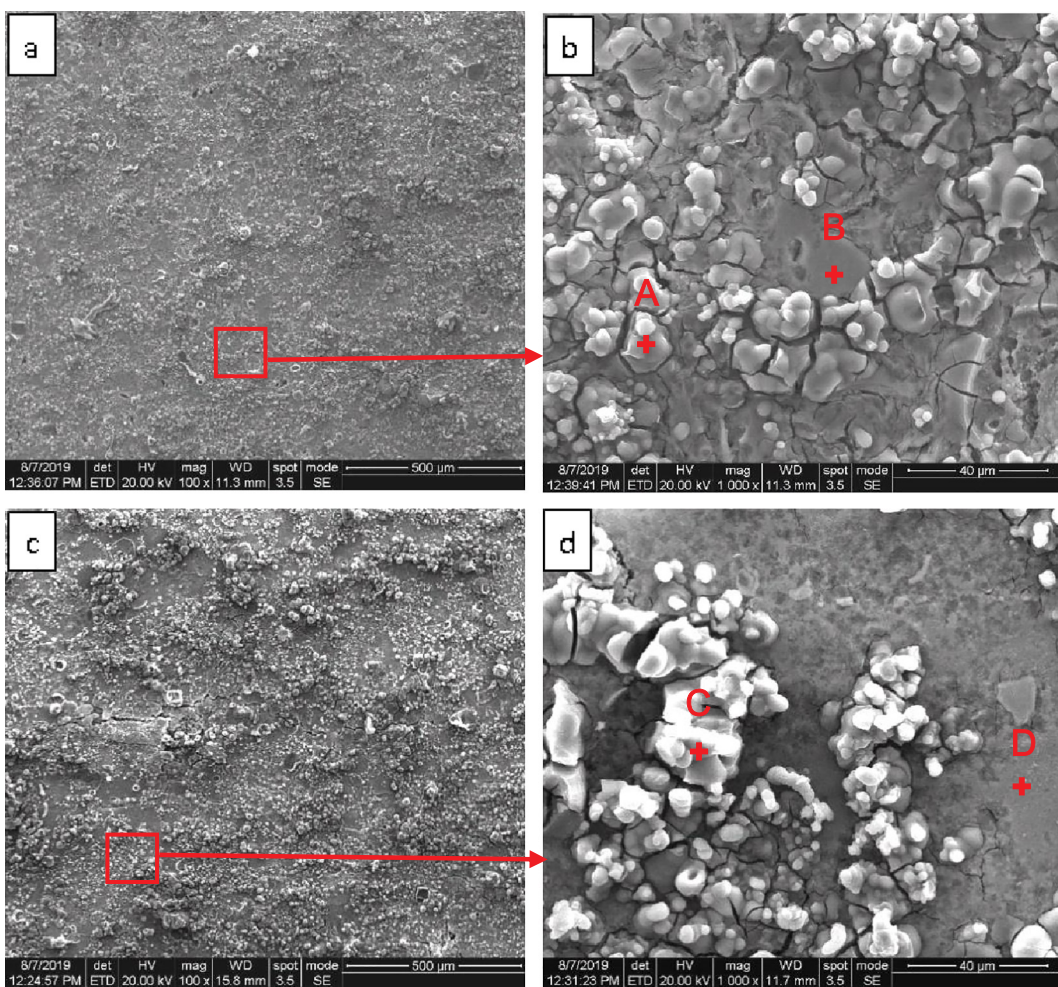


Fig. 10. SEM images of surfaces of uncoated 7075 aluminum alloys after electrochemical corrosion tests: (a, b) cold sprayed 7075 aluminum; (c, d) rolled 7075 aluminum (T6).

Table 5
EDS results of the corroded surfaces in Fig. 10.

Point	Elemental fraction (wt%)					
	Al	O	Mg	Zn	Cl	Na
A	41.22	53.18	1.53	2.50	1.57	–
B	85.10	4.95	2.98	6.43	0.30	0.24
C	39.84	55.01	1.64	1.05	1.84	0.61
D	76.58	11.06	3.11	8.94	0.31	–

observable in Table 3 that both the 7075 aluminum alloys with PEO coatings exhibited much better corrosion resistance with much lower corrosion current density and higher R_p values than those of the uncoated samples. Besides this, the corrosion potentials of both of the coated samples were nobler than uncoated samples, implying a weaker tendency to corrode in chloride solution. It can be noticed in Fig. 7 that all the PEO coated 7075 aluminum alloy samples obtained favorable electrochemical resistance in NaCl containing environment, with a slow corrosion rate and a high polarization resistance value especially in case of the as-sprayed alloy, the corrosion current density was only $1.16 \times 10^{-4} \text{ A/cm}^2$; while the uncoated samples showed undesirable corrosion behavior.

3.4. Wear resistance

The curves of the coefficient of friction of the PEO coated and

uncoated alloys recorded during sliding wear tests were plotted against the sliding time as shown in Fig. 8. The coefficient of friction of the coated samples increased rapidly for 5 min at the beginning after which it got raised a little bit and became steady within the 0.64 to 0.68 range with small fluctuations as observed in Fig. 8. In the case of the cold sprayed and rolled 7075 aluminum alloy samples, the coefficient of friction curve increased to 0.57 within the initial 5 min, and then it dropped to 0.4, and subsequently, it got stabilized between 0.35 and 0.5 with moderate fluctuations. The cross-sectional profiles of wear tracks of the cold sprayed and rolled 7075 aluminum alloys before and after PEO treatment are shown in Fig. 9. These cross-sectional wear profiles were used to calculate the material loss quantitatively, and their average coefficient of friction were obtained from Fig. 8. The summary of the wear test results is shown in Table 4. From Table 4, it can be inferred that the wear rates of coated samples were two orders lower than those without coatings for both the cold sprayed and the rolled 7075 aluminum alloys. It is inferred that, the volumetric wear rate of the cold sprayed sample with PEO coating is $1.22 \times 10^{-6} \text{ mm}^3/\text{N}\cdot\text{m}$, is slightly lower compared to the rolled one with PEO coating ($3.30 \times 10^{-6} \text{ mm}^3/\text{N}\cdot\text{m}$).

4. Discussion

4.1. Mechanical properties of the cold sprayed aluminum alloy and PEO coatings

Bulk-scale mechanical properties of CS deposits are mainly

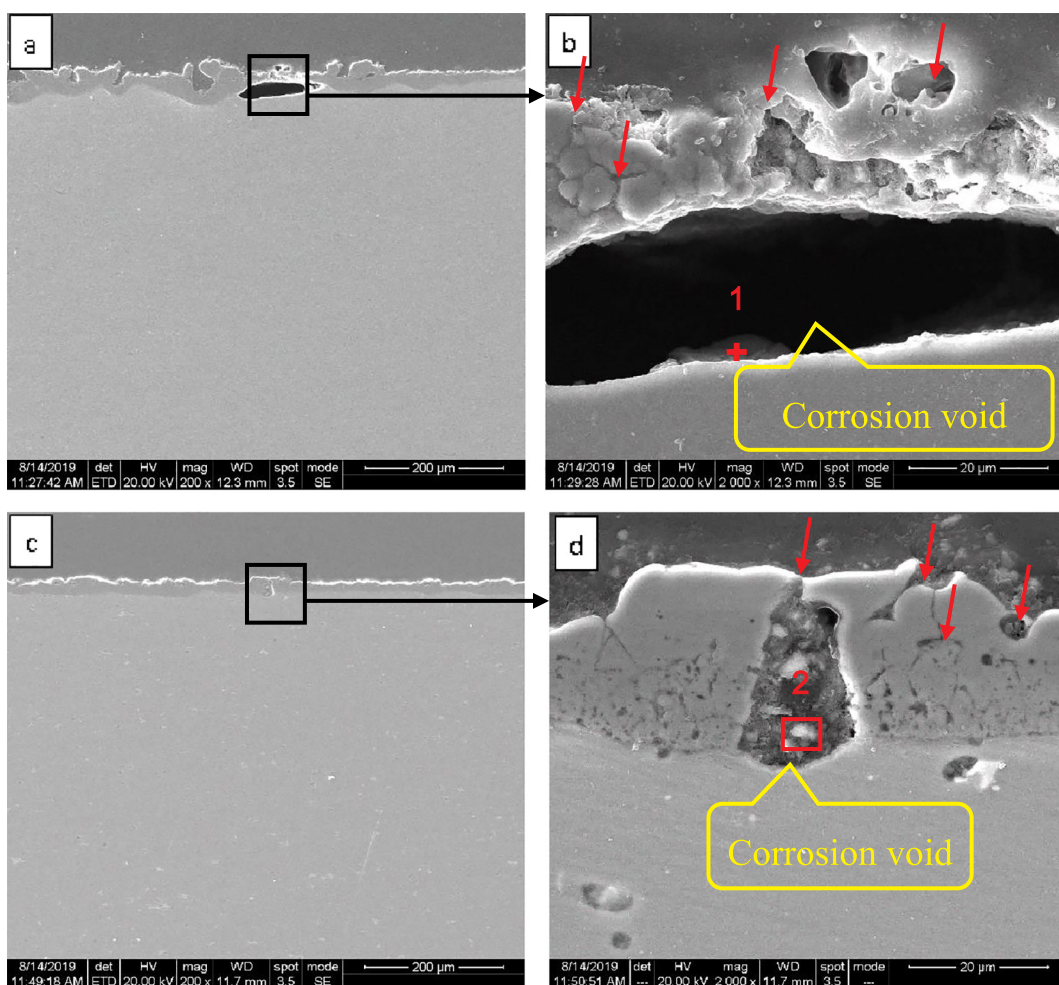


Fig. 11. Cross-sectional SEM morphologies of coated 7075 aluminum alloy s after electrochemical corrosion tests: (a, b) cold sprayed 7075 aluminum; (c, d) rolled 7075 aluminum (T6).

Table 6

EDS results of points 1 and 2 on cross-sections of corroded cold sprayed 7075 aluminum alloy from Fig. 11.

Point	Elemental fraction (wt%)					
	Al	O	Mg	Zn	Cl	Na
1	48.91	44.35	1.15	4.43	0.28	0.27
2	66.41	25.51	2.02	5.52	0.55	–

determined by particle impact velocity and particle impact temperature, and any parameters which influence these factors would affect the final mechanical properties of the cold sprayed material, including microhardness, bond strength, tensile strength and ductility, conductivity, residual stress, fatigue and corrosion [38]. There is an ideal range of particle impact velocity and temperature to obtain optimal mechanical properties of CS deposits. The cold sprayed aluminum alloy usually displays satisfactory microhardness and ultimate tensile strength, although they are not comparable with those of post heat treated ones. The elongation to fracture value of the as-deposited 7075 aluminum in this study was only 2.9%. This reduction in elongation was caused by the extensive cold work introduced into the microstructure during CS deposition. The presence of inherent defects in CS deposits, such as porosities and inferior bonding between the particle boundaries, would cause low electrical conductivity [8,38], which may influence the micro-arc discharge during the PEO process. These defects were found in this study as seen in Fig. 5(a) (inset image). The particles

which underwent excessive cold work during impact reduced the ductility of the deposit. However, these defects can be abridged by adopting suitable heat treatments, which will in turn improve the mechanical properties. Rokni et al. [18] performed several heat treatments on as-deposited CS coatings, which significantly increased the ultimate tensile strength and microhardness of the samples to ~560 MPa (T73) and 189 HV_{0.3} (T6), respectively. The elongation at fracture value was improved to near 6%. These improved mechanical properties are close to those of the conventional wrought 7075 Al alloys after heat treatments [39,40]. Among the mechanical properties of the PEO coatings, microhardness was given the most attention in the investigation, which was decisively affected by its phase composition and microstructure. Generally, an alumina coating with a dense microstructure with high amounts of α -Al₂O₃ phase would show higher microhardness. It was observed that the pancake structures are formed in the PEO deposit due to the rapid solidification of molten alumina [41]. Within these pancake structures, there were shrinkage cavities located at the apexes of discharge channels formed due to the rapid quenching occurring during the process. The stacking faults created during the formation of these pancake structures led to the creation of porous features in the PEO coating [42]. The much noticeable micro-cracks are thought to be resulting from the thermal stress generated during the rapid cooling of newly generated alumina lamellae [31]. Concerning the phase composition, the integrated intensities of the (113) α -Al₂O₃ (43.36° in 2θ) and (400) γ -Al₂O₃ (45.84° in 2θ) peaks in the XRD patterns represent the relative content of α -Al₂O₃ and γ -Al₂O₃ respectively in the coatings [43]. However, the (113) α -Al₂O₃ peak did not show up in the XRD

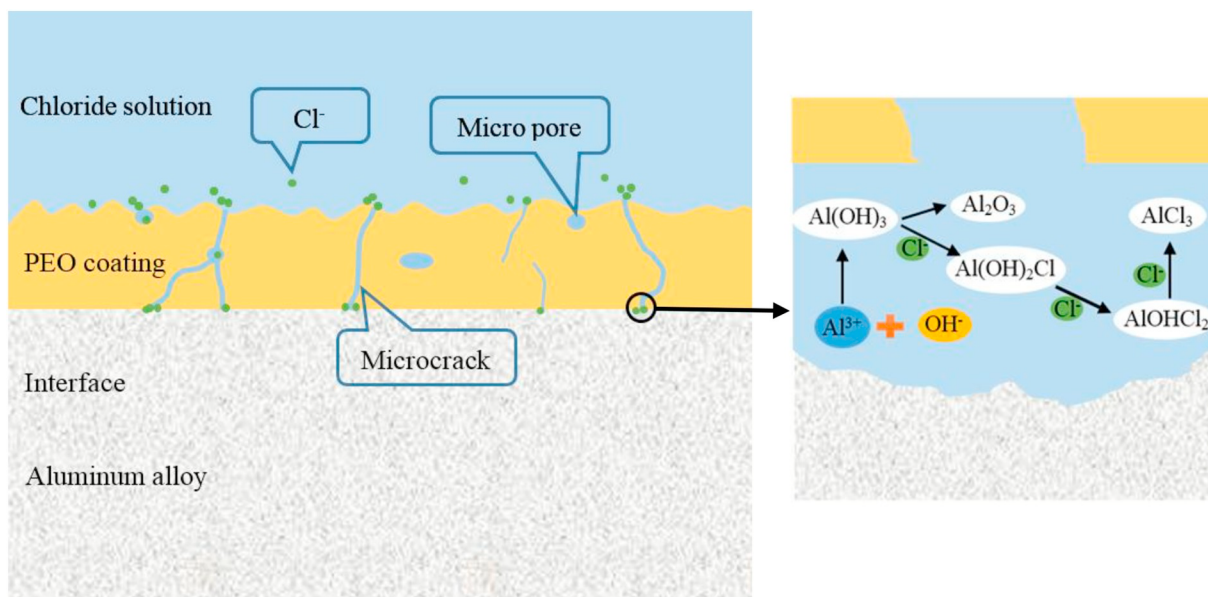


Fig. 12. Cross-sectional schematic of the electrochemical corrosion process in chloride solution for coated 7075 aluminum alloy.

pattern because the formation of $\alpha\text{-Al}_2\text{O}_3$ was suppressed by alloying elements of Zn [44] and Mg [45]. It must be noted that the main alloying element in 7075 aluminum alloy is the 'Zn,' which decisively affects the phase transformation [44]. The relative phase contents are also affected by the electrical parameters and the treatment/processing time used in the PEO process [43]. Sundararajan et al. [46] proposed that there is supposed to be more $\alpha\text{-Al}_2\text{O}_3$ phase content within a thicker coating compared to a thinner coating. Therefore, the thin coating fabricated in the present study exhibited a small proportion of $\alpha\text{-Al}_2\text{O}_3$. Albeit the two PEO coatings had the same phase composition, their microstructure and resultant microhardness were different. Compare with the rolled sample, the PEO coating fabricated on the cold sprayed sample possessed better quality characterized by its more uniform thickness distribution and lower degree of defects, including micropores, microcracks, and huge craters. The numerous huge craters on the PEO coating produced on the rolled 7075Al alloy sample are supposed to be associated with its better electrical conductivity than the cold sprayed one since the huge craters derived from strong micro-arc discharges. It can be deduced that the presence of different degree of defect features in the two coatings may be related to the different electrical conductivity and temper difference (as-sprayed condition and T6 condition) between their substrates, but this phenomenon is still ambiguous. The 7075 aluminum CS deposit obtained in this study exhibited acceptable mechanical properties, and after subjecting it to the PEO surface treatment, its wear and corrosion performance were greatly improved. These results indicate that the PEO treated CS deposit has the potential to be applied in restoration of damaged components and fabrication of individual components. It can be put to use where the mechanical performance is not very demanding where as high corrosion and wear resistance are desired. One good example for the aforementioned application is the aluminum flange sprayed on an aluminum pipe.

4.2. Electrochemical corrosion mechanism

The corrosion test results show that without the protection of the PEO coating, the corrosion current densities of uncoated samples reached values higher than 0.01 A/cm^2 during the anodic polarization, which means high rate of dissolution of aluminum alloy and generation of more number of Al^{3+} ions. For the uncoated samples, it was observed that when the polarization reached closer to the corrosion potentials,

the anodic current density suddenly gets shifted to higher values, forming a horizontally aligned line on the polarization curves. This results in the formation of pits on the electrode, aided by the creation of air bubbles surrounding the electrodes. This phenomenon is designated as pitting potential, and similar observations have been reported elsewhere [37,47]. In the present study, such a pitting phenomenon was not observed on the PEO treated samples, implying the effectiveness of the protection offered by the Al_2O_3 coating generated during the PEO process. Without the protection of PEO coatings, the surfaces of the uncoated samples were severely corroded and covered with massive corrosion products, as seen in Fig. 10. The EDS results of points A, B, C, and D shown in Fig. 10 (b) and (d) are summarized in Table 5. From Table 5, it is clear that the corrosion products contain more oxygen element (point A and C), and it is indicative of the existence of $\text{Al}(\text{OH})_3$ or its subsequent products. In neutral NaCl solution, the reaction can be described as follows [48]:



The white precipitate of $\text{Al}(\text{OH})_3$ may undergo a secondary reaction to produce Al_2O_3 , or react with the adsorbed Cl^- to produce $\text{Al}(\text{OH})_2\text{Cl}$, AlOHCl_2 and AlCl_3 continuously. It is noticeable that the electrochemical behavior of the rolled aluminum alloy was better than the cold sprayed material since the corrosion density value of the former was lower. This difference between the two materials can be ascribed to their different degree of plastic deformation. The as-sprayed aluminum alloy underwent severe plastic deformation and provided more active sites for corrosion [36]. The Al_2O_3 ceramic coating is chemically stable and functions as a barrier between the substrate and the corrosive solution [49–51]. The PEO coating can effectively suppress the Cl^- transfer through the coating and can prevent it from contacting the aluminum alloy. However, the presence of the micro-cracks and pores can provide the pathways for electrolytes to penetrate into the interface between PEO coating and 7075 aluminum substrate, causing subsequent corrosive attack (Fig. 11). Red arrows, which are shown in Fig. 11(b, d) denotes these pathways. As mention previously in the microstructure analysis of the PEO coatings, the coating fabricated on the cold sprayed aluminum alloy was less defective and relatively thicker than that formed on the rolled sample; thus there were fewer pathways in the PEO coating formed on the cold sprayed sample for penetration of the corrosive solution. Also, thin areas of the huge craters in the rolled sample became the weak spots, which are vulnerable to corrosion attack. For the PEO coated samples, the calculated R_p

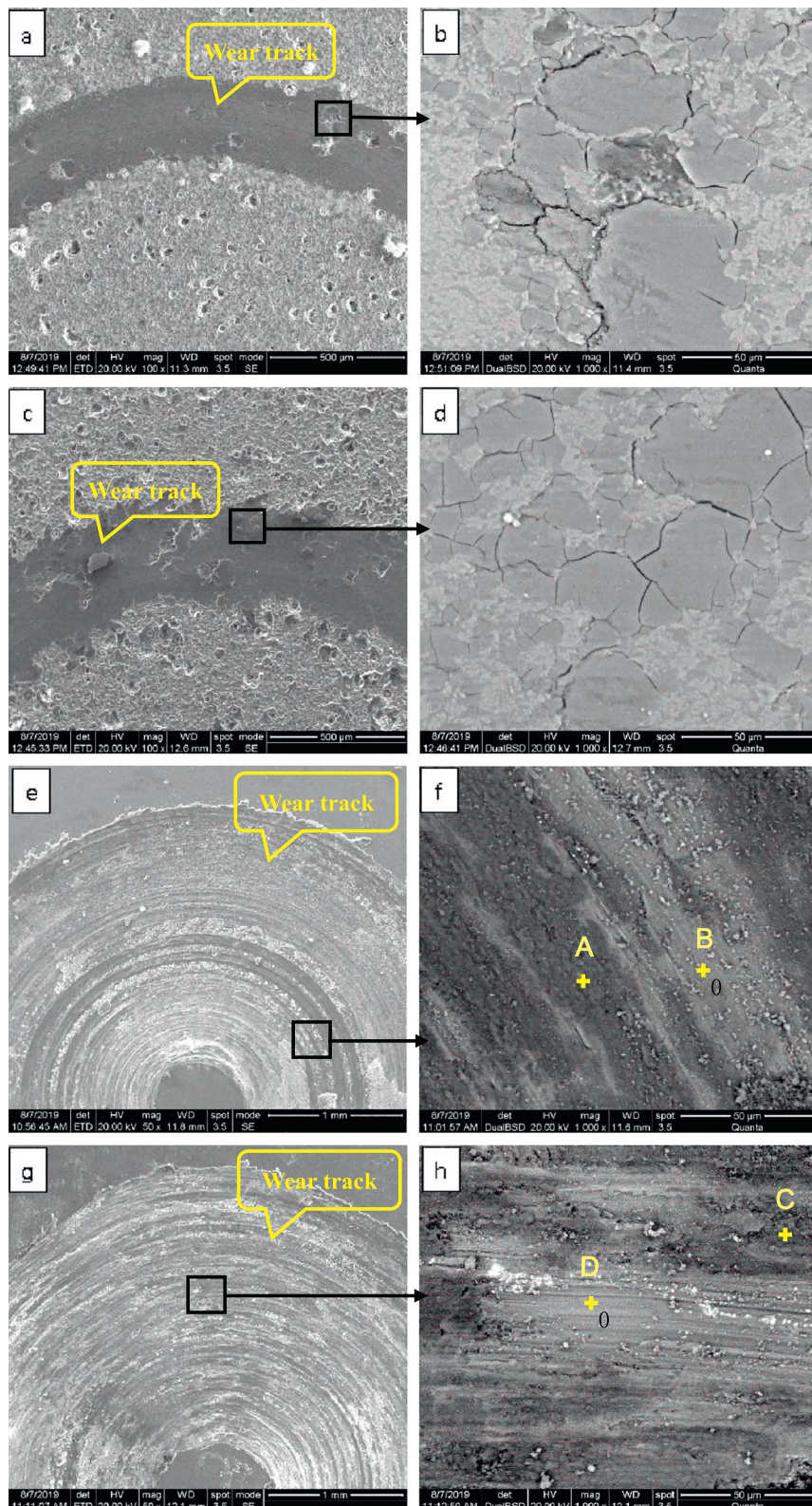


Fig. 13. SEM images of wear track appearances for (a, b) coated cold sprayed 7075 aluminum alloy; (c, d) coated rolled 7075 aluminum alloy; (e, f) uncoated cold sprayed 7075 aluminum alloy; (g, h) uncoated rolled 7075 aluminum alloy.

value of the cold sprayed sample was 2.5 times higher compared to that of the rolled sample, reflecting a more outstanding corrosion resistance. The EDS results of points 1 and 2 in Fig. 11 (b, d) are listed in Table 6. From Table 6, the elements Cl and Na can be found in the corrosion voids of the two PEO coatings. It is clear that the corrosive media has

penetrated the interface through the corrosion pathways. The corrosion action between the coating and alloy substrate has resulted in the dissolution of cold sprayed 7075 aluminum alloy, leading to the creation of corrosion voids. The corrosion performance of the alumina coating is determined by several factors, including coating microstructure, phase

Table 7

EDS results of point A and B of wear track on the as-sprayed 7075 aluminum alloys displayed in Fig. 13(f, h).

Point	Elemental fraction (wt.%)			
	O	Al	Mg	Zn
A	35.99	57.92	04.00	02.09
B	02.94	88.75	03.00	05.31
C	27.76	66.60	02.29	03.35
D	00.74	90.37	02.95	05.94

composition, and density. Generally, a denser, thicker and chemically stable surface would provide more effective protection during the corrosion process by slowing down the diffusion rate of Cl^- within the layer [52]. This corrosion process of the cold sprayed 7075 aluminum alloy with PEO coating is illustrated in the schematic diagram shown in Fig. 12. In the present study, the alumina coatings formed on the cold sprayed 7075 aluminum fabricated in the aluminate electrolyte were relatively thicker, and it had fewer micro-cracks and micro-pores compared to the rolled one, and this can explain the better corrosion resistance of cold sprayed alloy after PEO treatment. Although the corrosion resistance of the cold sprayed and rolled 7075 aluminum can be significantly improved by PEO treatment, there were still traces of slight corrosion that had taken place at the interface between the PEO coating and 7075 aluminum substrate. Therefore, the post-treatment strategies, such as sealing and electrolytic plating, should be applied to the PEO coating to further improve the corrosion resistance of the PEO coatings, these aspects will be investigated in the near future.

4.3. Wear mechanism

The micro-morphologies of the wear tracks of the cold sprayed and rolled 7075 aluminum alloys before and after PEO treatment are shown in Fig. 13. From Figs. 13 and 9, it was found that the wear tracks of PEO coated samples were much smaller both in width and depth, which indicates a lower material loss, and this can be attributed to the PEO coating's composition, which was mainly comprised of Al_2O_3 , a ceramic much harder than 7075 aluminum alloy. It can be easily observed that smoother wear tracks without any evidence of accumulated deposits on the worn surfaces were obtained for the PEO coated samples when compared to the uncoated samples. During the wear process, the rubbing action between the Al_2O_3 coating and the paired Al_2O_3 ball eliminated the asperities and smoothened the contact surfaces, by generating just a small amount of fine debris, these debris got trapped within the wear track and were ground into much finer debris thereby contributing to the abrasive wear [51].

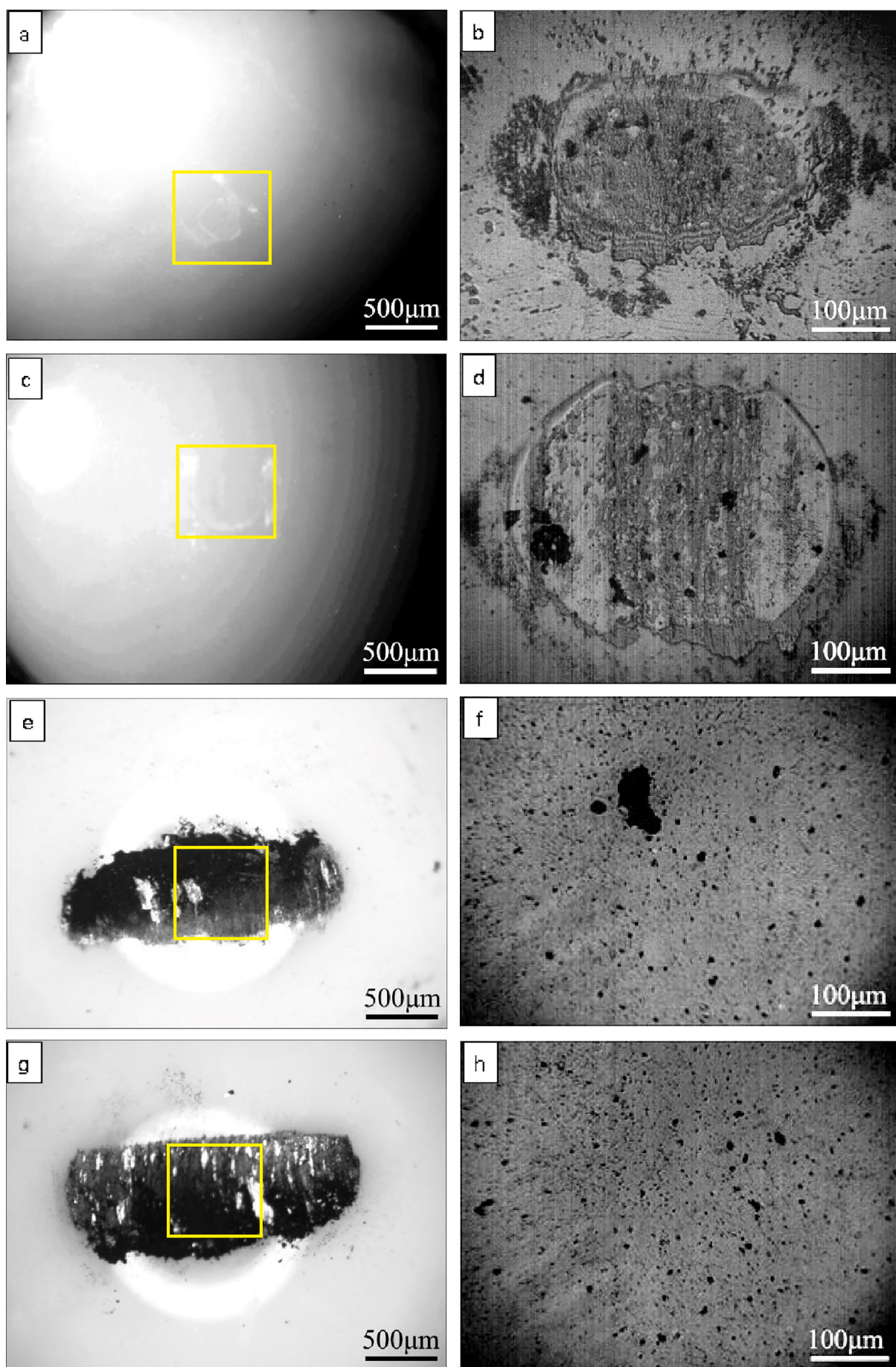
Although the surfaces of the PEO coatings were ground and polished before wear tests, the micropores and ends of microcracks remained on their surfaces, as can be seen beside the wear tracks in Fig. 13(a, c). The wear tracks on the PEO coating exhibit a flaky morphology with numerous randomly distributed microcracks (Fig. 13(b, d)), indicating the existence of fatigue wear in this experiment [53,54], and this phenomenon was also found by Xie et al. in their research on the wear performance of PEO treated A356 aluminum alloy [47]. These fatigue cracks may nucleate in-situ from the defects present inside the coatings. These fatigue cracks have high tendency to propagate under repeated impacts [55]. The microhardness of Al_2O_3 coating also plays a significant role in wear resistance, and high hardness is desirable for obtaining a wear-resistant surface [56]. Therefore, the relatively lower wear rate of cold sprayed 7075 aluminum alloy covered with the PEO coating can be associated with its lower degree of defects and resultant higher hardness compared to the coating that was formed on the rolled alloy. It is worth mentioning that the PEO coatings survived the whole test and did not wear out. The wear tracks of uncoated samples (Fig. 13(e, g)) are much rougher, and there is more wear debris that

remained, accumulated and formed a barrier in front of the direction of motion of the Al_2O_3 ball. This result may explain the more scattered coefficient of friction curve for the uncoated samples throughout the testing period [28]. The aluminum alloys were severely plowed due to the micro-cutting wear mechanism [47]. Also, the relatively high COFs observed at the beginning of wear test is associated to the material loss of the uncoated alloys generated by micro-cutting and delamination supported by plastic deformation, which resulted in great frictional force as seen in Fig. 8 [56]. The subsequent sudden drop of COFs of uncoated samples was caused by the rapid increase in the contact area of the tribo-couple. As the wear action continued, the aluminum alloys sustained a relatively stable friction force. During the wear process, massive wear debris got generated by micro-cutting and grinding actions. Some of the debris got evacuated from the friction path, while some got entrapped between the contact surfaces.

The captured debris got repeatedly ground, and thus the contact area was lubricated [30]. The lubrication effect along with smaller deformation force of aluminum alloy resulted in a lower coefficient of friction [57]. The EDS results of point A, B from Fig. 13(f) and point C, D from Fig. 13(h) are listed in Table 7. From Table 7, it is found that there is a significant difference in oxygen content. The darker areas from Fig. 13(f, h), represented by oxygen-rich points A and C, are tribofilms formed during wear process, which signifies a tribo-chemical wear mechanism [37]. The difference between the two wear processes will be compared further. Fig. 14 shows the optical images of the contact areas of Al_2O_3 balls paired with cold sprayed and rolled alloys, with and without PEO coatings respectively. The images on the right side are of higher magnification after rinsing. From the lower magnification images shown in Fig. 14, it is observable that negligible debris remained on the Al_2O_3 balls paired with coated samples while massive dark debris along with some bright splats were found to be adhered to those paired with uncoated samples. The bright splats seen in Fig. 14(e, g) were newly delaminated splats from the alloy surface, and the dark debris may be the repeatedly crushed and oxidized wear debris. The other wear debris collected from uncoated samples exhibited blocky particles (Fig. 15). Form Fig. 15, it can be found that the partial oxidation of the aluminum alloy wear debris was verified by the atomic percentage ratio of oxygen/aluminum ($\sim 51/45$) derived from the EDS results. Images at higher magnification (Fig. 14(b, d)) shows that wear scars formed on the contact area of Al_2O_3 balls paired well with the coated samples, whereas the Al_2O_3 balls paired with uncoated samples remained almost unscratched with a little amount of debris embedded in contact areas. Compared to 7075 aluminum alloy, the hardness of alumina coating is much higher and close to Al_2O_3 ball, thereby abrasion between the tribo-couple (Al_2O_3 ball/PEO coating) is mutual, as evidenced by the extended wear scars detected on the alumina balls paired with coated samples. Similar damage to Al_2O_3 ball was also observed when it was paired with an air plasma-sprayed Al_2O_3 coatings [58]. Based on the discussion above, the cross-sectional schematics are postulated to offer a better understanding of the different contact conditions of tribo-couples (Fig. 16). The deep wear track formed on the uncoated alloy with a distinct deformed area, and a rougher surface aided by the plowing effect, and the paired alumina ball remained almost intact (Fig. 16(a)). However, it was found that the wear process caused visible damage to the alumina ball paired with PEO coating (Fig. 16(b)). The smaller contact area and higher interfacial shear strength formed on the tribo-couple of Al_2O_3 ball/PEO coating resulted in a higher friction force and higher COFs. High friction force may induce fracture on the tested material [59], and this may explain the cracks formed on the worn surfaces of coated samples shown in Fig. 13(b, d).

5. Conclusions

- 1) The cold sprayed 7075 aluminum alloy exhibits favorable mechanical properties, with a density of 2.78 g/mm^3 , a hardness of



(caption on next page)

Fig. 14. Optical images of the Al_2O_3 balls paired with: (a, b) cold sprayed 7075 aluminum with PEO coating; (c, d) rolled 7075 aluminum with PEO coating; (e, f) cold sprayed 7075 aluminum without PEO coating; (g, h) rolled 7075 aluminum without PEO coating.

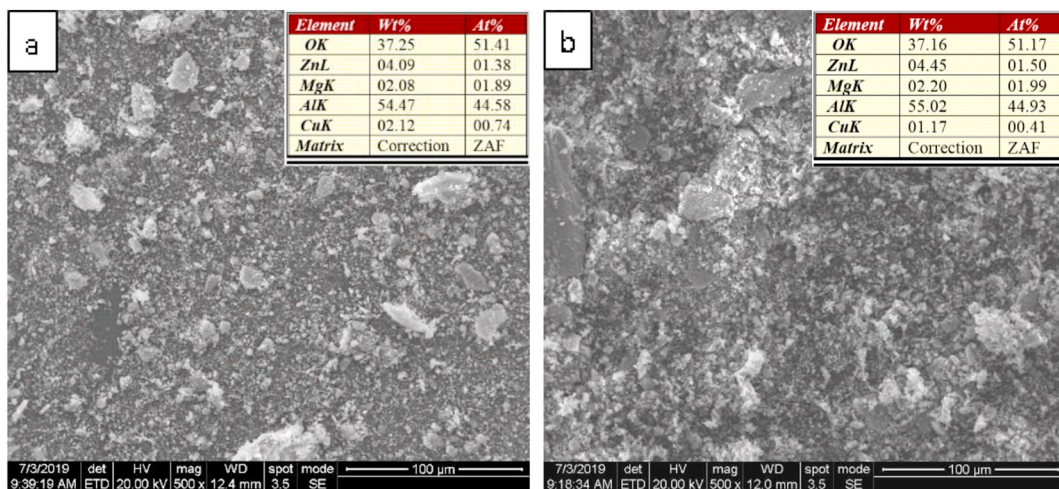


Fig. 15. Morphologies of wear debris of uncoated samples with EDS results: (a) cold sprayed 7075 aluminum without PEO coating; (b) rolled 7075 aluminum without PEO coating.

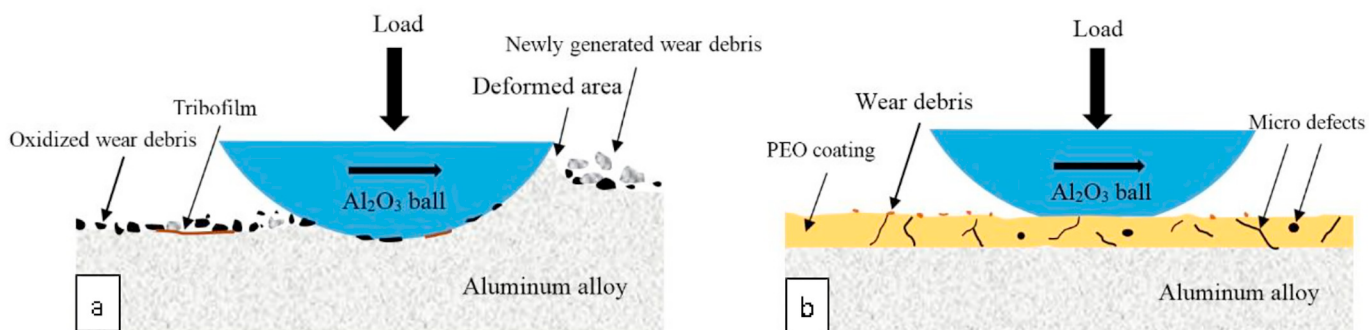


Fig. 16. Cross-sectional schematics of contact conditions of tribo-couples during wear process: (a) Al_2O_3 ball-aluminum alloy; (b) Al_2O_3 ball- Al_2O_3 coating.

- 144 HV_{0.3}, and an ultimate tensile strength of 395 MPa, except for its low elongation (2.9%).
- 2) The present coating formed on cold sprayed 7075 aluminum alloy in aluminate electrolyte has $\gamma\text{-Al}_2\text{O}_3$ as the primary phase, accompanied by a small amount of $\alpha\text{-Al}_2\text{O}_3$, with a thickness of ~15–20 μm, a hardness of 1353 HV_{0.01}, and a bond strength of over 38 MPa.
 - 3) The electrochemical corrosion resistance of the cold sprayed 7075 aluminum alloy was remarkably improved by PEO treatment, with three-order lowered corrosion current density and more noble corrosion potential. The microstructure of the coating decisively affects its capability of impeding a corrosive attack.
 - 4) The wear resistance of the cold sprayed 7075 aluminum alloy was substantially improved by PEO treatment, with a two-order lowered wear rate. The PEO coating survived a two-hour sliding wear test under a load of 5 N and a distance of 720 m. The high wear resistance of the layer can be attributed to its high hardness and compactness.
 - 5) High strength aluminum alloy having excellent chemical stability and high-hardness can be obtained by using cold spray process coupled with PEO treatment. Such alloys have tremendous potential to be applied for repairing the damaged parts or to manufacture new aluminum alloy components meant for textile industries.

Author contributions selection

Yuqin Rao: Investigation, Data curation, Writing - Original Draft
Qun Wang: Supervision, Project administration, Funding acquisition
Daisuke Oka: Resources, Data curation
Chidambaram Seshadri Ramachandran: Writing - Review & Editing

Declaration of competing interest

The authors declare that they have no known competing financial interests or personal relationships that could have appeared to influence the work reported in this paper.

Acknowledgments

This work was financially supported by the Changsha Science and Technology Project (No. kq 1801004) and the Natural Science Foundation of Hunan Province (2019JJ40045).

References

- [1] R.N. Raoelison, C. Verdy, H. Liao, Cold gas dynamic spray additive manufacturing today: deposit possibilities, technological solutions and viable applications, Mater.

- Des. 133 (2017) 266–287.
- [2] R.N. Raefelson, Y. Xie, T. Sapanathan, M.P. Planche, R. Kromer, S. Costil, et al., Cold gas dynamic spray technology: a comprehensive review of processing conditions for various technological developments till to date, *Addit. Manuf.* 19 (2018) 134–159.
- [3] A. Sova, S. Grigoriev, A. Okunkova, I. Smurov, Potential of cold gas dynamic spray as additive manufacturing technology, *Int. J. Adv. Manuf. Technol.* 69 (2013) 2269–2278.
- [4] N.H. Tariq, L. Gyansah, X. Qiu, H. Du, J.Q. Wang, B. Feng, et al., Thermo-mechanical post-treatment: a strategic approach to improve microstructure and mechanical properties of cold spray additively manufactured composites, *Mater. Des.* 156 (2018) 287–299.
- [5] W. Li, K. Yang, S. Yin, X. Yang, Y. Xu, R. Lupoi, Solid-state additive manufacturing and repairing by cold spraying: a review, *J. Mater. Sci. Technol.* 34 (2018) 440–457.
- [6] C. Borchers, F. Gärtner, T. Stoltenhoff, H. Assadi, H. Kreye, Microstructure and macroscopic properties of cold sprayed copper coatings, *J. Appl. Phys.* 93 (2003) 10064–10070.
- [7] T. Hussain, Cold spraying of titanium: a review of bonding mechanisms, microstructure and properties, *Key Eng. Mater.* 533 (2013) 53–90.
- [8] V. Champagne, D. Helfritch, The unique abilities of cold spray deposition, *Int. Mater. Rev.* 61 (2016) 437–455.
- [9] S. Yin, P. Cavaliere, B. Aldwell, R. Jenkins, H. Liao, W. Li, et al., Cold spray additive manufacturing and repair: fundamentals and applications, *Addit. Manuf.* 21 (2018) 628–650.
- [10] X. Luo, C.S. Ramachandran, G.J. Yang, Micro-nanostructured cermet coatings, *Advanced Nanomaterials and Coatings by Thermal Spray*, Elsevier, 2019, pp. 61–117.
- [11] P. Cavaliere, L. Cavaliere, *Cold-spray Coatings*, Springer, 2018.
- [12] <http://www.plasma.co.jp/en/products/coldspray.html>.
- [13] J. Henao, A. Conculstell, I.G. Cano, S. Dosta, N. Cinca, J.M. Guilemany, et al., Novel Al-based metallic glass coatings by cold gas spray, *Mater. Des.* 94 (2016) 253–261.
- [14] M.R. Rokni, C.A. Widener, O.C. Ozdemir, G.A. Crawford, Microstructure and mechanical properties of cold sprayed 6061 Al in As-sprayed and heat treated condition, *Surf. Coat. Technol.* 309 (2017) 641–650.
- [15] M.R. Rokni, C.A. Widener, V.K. Champagne, G.A. Crawford, Microstructure and mechanical properties of cold sprayed 7075 deposition during non-isothermal annealing, *Surf. Coat. Technol.* 276 (2015) 305–315.
- [16] R. Ghelichi, D. MacDonald, S. Bagherifard, H. Jahed, M. Guagliano, B. Jodoin, Microstructure and fatigue behavior of cold spray coated Al5052, *Acta Mater.* 60 (2012) 6555–6561.
- [17] A.G. Gavras, D.A. Lados, V.K. Champagne, R.J. Warren, Effects of processing on microstructure evolution and fatigue crack growth mechanisms in cold-spray 6061 aluminum alloy, *Int. J. Fatigue* 110 (2018) 49–62.
- [18] M.R. Rokni, C.A. Widener, V.K. Champagne, G.A. Crawford, S.R. Nutt, The effects of heat treatment on 7075 Al cold spray deposits, *Surf. Coat. Technol.* 310 (2017) 278–285.
- [19] P. Sirvent, M.A. Garrido, C.J. Muñez, P. Poza, S. Vezzu, Effect of higher deposition temperatures on the microstructure and mechanical properties of Al 2024 cold sprayed coatings, *Surf. Coat. Technol.* 337 (2018) 461–470.
- [20] P. Vo, E. Irissou, J.G. Legoux, S. Yue, Mechanical and microstructural characterization of cold-sprayed Ti-6Al-4V after heat treatment, *J. Therm. Spray Technol.* 22 (2013) 954–964.
- [21] N.H. Tariq, L. Gyansah, X. Qiu, H. Du, J.Q. Wang, B. Feng, et al., Thermo-mechanical post-treatment: a strategic approach to improve microstructure and mechanical properties of cold spray additively manufactured composites, *Mater. Des.* 156 (2018) 287–299.
- [22] M. Imran, A.A. Khan, Characterization of Al-7075 metal matrix composites: a review, *J. Mater. Res. Technol.* 8 (2019) 3347–3356.
- [23] P.A. Rometsch, Y. Zhang, S. Knight, Heat treatment of 7xxx series aluminium alloys—some recent developments, *Trans. Nonferrous Met. Soc. China* 24 (2014) 2003–2017.
- [24] A. Azarniya, A.K. Taheri, K.K. Taheri, Recent advances in ageing of 7xxx series aluminum alloys: a physical metallurgy perspective, *J. Alloy. Compd.* 781 (2018) 945–983.
- [25] K. Mistry, M. Priest, S. Shrestha, The potential of plasma electrolytic oxidized eutectic aluminium-silicon alloy as a cylinder wall surface for lightweight engine blocks, *Proc. Inst. Mech. Eng. J* 224 (2010) 221–229.
- [26] Y. Erarslan, Wear performance of in-situ aluminium matrix composite after micro-arc oxidation, *Trans. Nonferrous Met. Soc. China* 23 (2013) 347–352.
- [27] M. Treviño, N.F. Garza-Montes-de-Oca, A. Pérez, M.A.L. Hernández-Rodríguez, A. Juárez, R. Colás, Wear of an aluminium alloy coated by plasma electrolytic oxidation, *Surf. Coat. Technol.* 206 (2012) 2213–2219.
- [28] S. Luo, Q. Wang, R. Ye, C.S. Ramachandran, Effects of electrolyte concentration on the microstructure and properties of plasma electrolytic oxidation coatings on Ti-6Al-4V alloy, *Surf. Coat. Technol.* 375 (2019) 864–876.
- [29] Y. Yang, L. Zhou, Improving corrosion resistance of friction stir welding joint of 7075 aluminum alloy by micro-arc oxidation, *J. Mater. Sci. Technol.* 30 (2014) 1251–1254.
- [30] Q.P. Tran, T.S. Chin, Y.C. Kuo, C.X. Jin, T. Trung, C. Van Tuan, et al., Diamond powder incorporated oxide layers formed on 6061 Al alloy by plasma electrolytic oxidation, *J. Alloys Compd.* 751 (2018) 289–298.
- [31] T. Arunellaiappan, S. Arun, S. Hariprasad, S. Gowtham, B. Ravisankar, N. Rameshbabu, Fabrication of corrosion resistant hydrophobic ceramic nanocomposite coatings on PEO treated AA7075, *Ceram. Int.* 44 (2018) 874–884.
- [32] T. Arunellaiappan, S. Arun, S. Hariprasad, S. Gowtham, B. Ravisankar, N. Rameshbabu, Fabrication of corrosion resistant hydrophobic ceramic nanocomposite coatings on PEO treated AA7075, *Ceram. Int.* 44 (2018) 874–884.
- [33] S.V. Egorkin, S.V. Gnedenvkov, S.L. Sinebryukhov, I.E. Vyalyi, A.S. Gnedenvkov, R.G. Chizhikov, Increasing thickness and protective properties of PEO-coatings on aluminum alloy, *Surf. Coat. Technol.* 334 (2018) 29–42.
- [34] R.H.U. Khan, A. Yerokhin, X. Li, H. Dong, A. Matthews, Surface characterisation of DC plasma electrolytic oxidation treated 6082 aluminium alloy: effect of current density and electrolyte concentration, *Surf. Coat. Technol.* 205 (2010) 1679–1688.
- [35] L.R. Krishna, P.S. Babu, M. Tak, D.S. Rao, G. Padmanabham, G. Sundararajan, Processing of ceramic and cermet composite coatings for strategic and aerospace applications, in: Y. Mahajan, J. Roy (Eds.), *Handbook of Advanced Ceramics and Composites*, Springer, Cham, 2019.
- [36] O. Meydanoglu, B. Jodoin, E.S. Kayali, Microstructure, mechanical properties and corrosion performance of 7075 Al matrix ceramic particle reinforced composite coatings produced by the cold gas dynamic spraying process, *Surf. Coat. Technol.* 235 (2013) 108–116.
- [37] Y. Tao, T. Xiong, C. Sun, H. Jin, H. Du, T. Li, Effect of α -Al₂O₃ on the properties of cold sprayed Al/ α -Al₂O₃ composite coatings on AZ91D magnesium alloy, *Appl. Surf. Sci.* 256 (2009) 261–266.
- [38] M.R. Rokni, S.R. Nutt, C.A. Widener, V.K. Champagne, R.H. Hrabe, Review of relationship between particle deformation, coating microstructure, and properties in high-pressure cold spray, *J. Therm. Spray Technol.* 26 (2017) 1308–1355.
- [39] J.F. Li, Z.W. Peng, C.X. Li, Z.Q. Jia, W.J. Chen, Z.Q. Zheng, Mechanical properties, corrosion behaviors and microstructures of 7075 aluminium alloy with various aging treatments, *Trans. Nonferrous Met. Soc. China* 18 (2008) 755–762.
- [40] S.K. Panigrahi, R. Jayaganthan, Effect of ageing on microstructure and mechanical properties of bulk, cryorolled, and room temperature rolled Al 7075 alloy, *J. Alloys Compd.* 509 (2011) 9609–9616.
- [41] L.R. Krishna, P.S. Babu, M. Tak, D.S. Rao, G. Padmanabham, G. Sundararajan, Processing of ceramic and cermet composite coatings for strategic and aerospace applications, in: Y. Mahajan, J. Roy (Eds.), *Handbook of Advanced Ceramics and Composites*, Springer, Cham, 2019.
- [42] G.B. Darband, M. Aliofkhazraei, P. Hamghalam, N. Valizade, Plasma electrolytic oxidation of magnesium and its alloys: mechanism, properties and applications, *J. Magnesium Alloys* 5 (2017) 74–132.
- [43] Y.L. Cheng, J.H. Cao, M.K. Mao, Z.M. Peng, P. Sheldon, G.E. Thompson, High growth rate, wear resistant coatings on an Al-Cu-Li alloy by plasma electrolytic oxidation in concentrated aluminate electrolytes, *Surf. Coat. Technol.* 269 (2015) 74–82.
- [44] Y. Gencer, A.E. Gulec, The effect of Zn on the microarc oxidation coating behavior of synthetic Al-Zn binary alloys, *J. Alloys Compd.* 525 (2012) 159–165.
- [45] Y.J. Oh, J.I. Mun, J.H. Kim, Effects of alloying elements on microstructure and protective properties of Al₂O₃ coatings formed on aluminum alloy substrates by plasma electrolysis, *Surf. Coat. Technol.* 204 (2009) 141–148.
- [46] G. Sundararajan, L.R. Krishna, Mechanisms underlying the formation of thick alumina coatings through the MAO coating technology, *Surf. Coat. Technol.* 167 (2003) 269–277.
- [47] H.J. Xie, Y.L. Cheng, S.X. Li, J.H. Cao, C.A.O. Li, Wear and corrosion resistant coatings on surface of cast A356 aluminum alloy by plasma electrolytic oxidation in moderately concentrated aluminate electrolytes, *Trans. Nonferrous Met. Soc. China* 27 (2017) 336–351.
- [48] J. Zhang, D. Kong, Effect of micro-arc oxidation on friction-wear behavior of cold-sprayed Al coating in 3.5% NaCl solution, *J. Mater. Eng. Perform.* 28 (2019) 2716–2725.
- [49] A.L. Yerokhin, X. Nie, A. Leyland, A. Matthews, S.J. Dowey, Plasma electrolysis for surface engineering, *Surf. Coat. Technol.* 122 (1999) 73–93.
- [50] Z. Ye, D. Liu, X. Zhang, Z. Wu, F. Long, Influence of combined shot peening and PEO treatment on corrosion fatigue behavior of 7A85 aluminum alloy, *Appl. Surf. Sci.* 486 (2019) 72–79.
- [51] A. Algahtani, E.R. Mahmoud, Erosion and corrosion resistance of plasma electrolytic oxidized 6082 aluminum alloy surface at low and high temperatures, *J. Mater. Res. Technol.* 8 (2019) 2699–2709.
- [52] N. Barati, A. Yerokhin, F. Golestanifar, S. Rastegari, E.I. Meletis, Alumina-zirconia coatings produced by plasma electrolytic oxidation on Al alloy for corrosion resistance improvement, *J. Alloys Compd.* 724 (2017) 435–442.
- [53] J. Takadoum, *Materials and Surface Engineering in Tribology*, John Wiley & Sons, 2013.
- [54] C.S. Ramachandran, V. Balasubramanian, P.V. Ananthapadmanabhan, V. Viswabaskaran, Understanding the dry sliding wear behaviour of atmospheric plasma-sprayed rare earth oxide coatings, *Mater. Des.* 39 (2012) 234–252.
- [55] C.S. Ramachandran, V. Balasubramanian, R. Varahamoorthy, Comparative evaluation of dry sliding wear behaviour of plasma transferred arc hardfaced surfaces by the pin-on-roller method, *Proc. Inst. Mech. Eng. J* 224 (2010) 91–106.
- [56] S.J. Cho, H. Moon, B.J. Hockey, S.M. Hsu, The transition from mild to severe wear in alumina during sliding, *Acta Metall. Mater.* 40 (1992) 185–192.
- [57] R. Gecu, Y. Yurekurt, E. Tekoglu, F. Muhaffel, A. Karaaslan, Improving wear resistance of 304 stainless steel reinforced AA7075 aluminum matrix composite by micro-arc oxidation, *Surf. Coat. Technol.* 368 (2019) 15–24.
- [58] Q. Wang, C.S. Ramachandran, G.M. Smith, S. Sampath, Sliding wear behavior of air plasma sprayed Al2O3 coatings sealed with aluminum phosphate, *Tribol. Int.* 116 (2017) 431–439.
- [59] R.R. Chromik, S.A. Alidokht, J.M. Shockley, Y. Zhang, Tribological coatings prepared by cold spray, *Cold-Spray Coatings*, Springer, Cham, 2018, pp. 321–348.